coatings

MDPI

Article

A Facile Two-Step PVP-Assisted Deposition of Co-Activated Nanosized Nickel Hydroxide Directly on a Substrate for Large-Scale Production of Supercapacitor Electrodes

Valerii Kotok [1,*], Peter Ondrejka [2], Miroslav Mikolášek [2,*], Michaela Sojková [3], Patrik Novák [4], Maroš Gregor [5], Vadym Kovalenko [6] and Kostyantyn Sukhyy [7]

1 General Chemical Technology Department, Ukrainian State University of Chemical Technology, 49005 Dnipro, Ukraine
2 Institute of Electronics and Photonics, Slovak University of Technology in Bratislava, 84104 Bratislava, Slovakia
3 Institute of Electrical Engineering, Slovak Academy of Sciences in Bratislava, 84104 Bratislava, Slovakia
4 Institute of Nuclear and Physical Engineering, Slovak University of Technology in Bratislava, 84104 Bratislava, Slovakia
5 Department of Experimental Physics, Faculty of Mathematics, Physics and Informatics Comenius University, 84248 Bratislava, Slovakia
6 Department of Analytical Chemistry and Chemical Technology of Food Additives and Cosmetics, Ukrainian State University of Chemical Technology, 49005 Dnipro, Ukraine
7 Department of Fuel, Polymer, and Polygraphic Materials Technologies, Ukrainian State University of Chemical Technology, 49005 Dnipro, Ukraine
* Correspondence: valeriykotok@gmail.com (V.K.); miroslav.mikolasek@stuba.sk (M.M.); Tel.: +380-636-604-828 (V.K.); +421-2-602-91-872 (M.M.)

Abstract: The self-decomposition reaction of the nickel ammonia complex was used for the nickel hydroxide formation on the nickel foam with further modification in several ways. The addition of polyvinyl pyrrolidone (PVP) and the electrochemical or chemical activation with cobalt hydroxide was used to modify the formation method. In all cases, structures with $Ni(OH)_2$ nanoflakes were formed. It was found that the flower-like particles of $Co(OH)_2$ were precipitated during chemical activation among the nanoflakes. It was shown that the presence of PVP during the nickel ammonia complex decomposition suppressed the highly branched particles. The absence of the highly branched particles increased the capacitive properties of the formed electrode at high current densities. The highest capacitance in 1408 F/g at 1 A/g was shown for the sample precipitated with the PVP presence and the further chemical activation by cobalt.

Keywords: nickel hydroxide; supercapacitor; cobalt hydroxide; polyvynilpyrllidone; nanoflakes

check for updates

Citation: Kotok, V.; Ondrejka, P.; Mikolášek, M.; Sojková, M.; Novák, P.; Gregor, M.; Kovalenko, V.; Sukhyy, K. A Facile Two-Step PVP-Assisted Deposition of Co-Activated Nanosized Nickel Hydroxide Directly on a Substrate for Large-Scale Production of Supercapacitor Electrodes. *Coatings* **2023**, *13*, 84. https://doi.org/10.3390/coatings13010084

Academic Editor: Emerson Coy

Received: 23 November 2022
Revised: 19 December 2022
Accepted: 22 December 2022
Published: 3 January 2023

1. Introduction

Aiming to reduce the human carbon footprint and influence on nature forces modern society to use renewable energy sources [1]. However, at the moment, autonomous energy storage is not possible without chemical power sources [2].

Nickel hydroxide (II) and relative materials are widely used as a component of alkaline battery electrodes [3]. The thin films of nickel hydroxides are potential materials for electrochromic devices [4–6]. The nickel hydroxide deposits formed on the different substrates have been applied for fuel cell electrodes [7–9], for the oxidation of pollutants [10–12] and for the detection of different molecules [13–15]. The powder of nickel hydroxide can be used for recycling plastic with hydrogen production [16]. The electrodes based on nickel hydroxide are also considered efficient for water splitting [17,18].

The reasons behind the high diversity of applications for $Ni(OH)_2$ include a high reversibility of reactions (1, 2), a high oxidation ability and the semiconducting properties of NiOOH.

$$\underset{\text{solid-state reaction}}{Ni(OH)_2 \rightarrow NiOOH + H^+ + 1e^-,} \quad (1)$$

$$\underset{\text{summary reaction}}{Ni(OH)_2 + OH^- \rightarrow NiOOH + H_2O + 1e^-,} \quad (2)$$

Nickel hydroxide and its related materials such as Ni-based layered double hydroxides (LDH) can be applied as electrode materials for hybrid supercapacitors (SCs). The main difference between supercapacitors (SC) and convenient secondary batteries is that SCs can be discharged and charged by much higher currents. This property can be used for starting electrical engines, pulse welding and other applications. A combination of an SC and a convenient battery can save space and weight [19] and extend the cycle life of a battery [20].

Nickel hydroxide and its relative materials are also used in hybrid supercapacitors. The capacitance of these materials consists of a pseudocapacitance (the faradaic reaction (1)) and a double-layer capacitance [21]. Therefore, for the successful application in SCs, these materials must have a high specific surface area and a high proton diffusion coefficient. On the other hand, a too-branched surface can prevent the running of an electrochemical reaction due to the resistance of the electrolyte and the material. This can be explained by the following equation for resistance R:

$$R = \rho \cdot l/S, \quad (3)$$

where ρ is the specific resistance in Ohm·cm and l and S are the length and the area of the pore/element of the material in cm and cm^2, respectively.

In the case of a very long pore (a nanosized element of an active material) and its small cross-sectional area, the final resistance will be so high that it suppresses the processes. Researchers need to avoid synthesizing extra branched materials with long and small pores.

Nevertheless, nanosized materials have been successfully synthesized and used for SC electrodes by many authors.

In [22], an active material was synthesized for SCs consisting of cobalt–nickel double hydroxide nanoflakes on nitrogen–doped hollow carbon spheres. The synthesis was carried out in two steps. For the synthesis, a complex procedure and a row of reactants were used. The optimized material demonstrated a specific capacitance of 578 C/g at 1 A/g as well as a good rate capacity of 76.54% at 1–20 A/g. The measurements were carried out for a pasted electrode.

The authors in [23] obtained composites based on carbon derived from tea leaves and covered by nickel hydroxide. It was prepared by using nickel nitrate hydrolysis at 110 °C for 12 h in an autoclave. The resulting precipitate was used for pasting the electrode forms. The capacitance of the optimized material was found to be 945 F/g at 1 A/g.

A two-step method for achieving Ni–doped tin disulfide@Nickel hydroxide directly on carbon cloth was proposed in [24]. First, the researchers carried out the formation of Ni-doped tin disulfide with the help of the hydrothermal method in the presence of several components. The precipitate formed on the carbon cloth was covered by the further hydrothermal formation of $Ni(OH)_2$. The resulting material demonstrated a capacitance of 2090 F/g at 1 A/g and good stability.

Another group of researchers [25] synthesized modified carbon nanotubes with cobalt and nickel hydroxide. The composites were obtained based on the matrix of the multiwall carbon nanotubes: non-functionalized (MWCNT). The synthesis was carried out as a simple chemical deposition. The physicochemical properties of the obtained nanocomposites were investigated with a focus on their use as the electrode materials of supercapacitors. The optimized material had a specific capacitance of 116 mF obtained using cyclic voltammetry for 10–80 mV/s sweep rates.

The $Ni(OH)_2$ flower-like particles were obtained directly on the ZnO substrate [26]. The researchers chose a facile one-step electrochemical method. The resulting electrodes showed excellent parameters: 2264.55 F/g at 0.5 A/g, a performance rate of 601.09 F/g at 30 A/g and a high cycle stability of 94.9% after 5000 cycles.

Another work dedicated to the nickel–manganese based composite on the substrate was presented in [27]. The authors synthetically formed the structure through the coprecipitation method. As a result, the developed structure had multilevel corrugations with more surface-active sites. The deposited active material demonstrated the highest capacitance of 2454 F/g at a current density of 1 A/g.

In [28], the researchers proposed a high-temperature two-step method for producing a flexible binder-free Ni–$Ni(OH)_2$/carbon nanofiber (CNF) composite material. This material was created using electrospinning followed by a high-temperature, hydrothermal and carbonization process. The best electrodes exhibited a capacitance of 763 F/g at a current density of 1 A/g and showed a cyclic stability of 94% after 8000 cycles.

A mixed material based on a copolymer of thiophene and pyrrole incorporated into a nickel hydroxide/nickel sulfide composite was synthesized via a complex multistage procedure [29]. The final precipitate in a mixture of the binder and the conductive additive was used for the pasted electrode preparation. A carbon cloth was used as a substrate. The electrodes demonstrated a high cycling stability. On the contrary, the capacitance was about 87 C/g at a current density of 1 A/g.

The group of researchers synthesized a material based on nickel hydroxide that was coated with carbon nanoparticles on a hybrid three-dimensional graphene foam [30]. The complex three-stage procedure included the modification of the nickel foam by forming the graphene and carbon nanoparticles and the electrodeposition of the nickel hydroxide. The ready-to-use electrodes demonstrated a high capacitance of 4667 F/g at 2 A/g.

The hollow nickel-cobalt-layered double hydroxide nanocages were obtained via a two-step synthesis with the help of several reagents. The proposed synthesis required heating. The precipitate was used for the pasted electrode formation. The paste contained a conductive additive and a binder. The Ni-Co LDH electrode showed a capacitance of 2369.0 F/g at 0.5 A/g and a good rate capability [31].

The $Ni(OH)_2$/g-C_3N_4 nanocomposite was grown by using a simple precipitation synthesis where the direct formation on the substrates was carried out. The optimized electrode showed 463 F/g in the next cyclic voltammetry mode: −300 to 500 mV (vs. SCE) at 10 mV/s [32].

In [33], the lanthanum-doped nickel hydroxide was shown with a capacitance of 1510.7 F/g at 1 A/g. The synthesis method required multiple components and heating up to 150 °C. The resulting precipitate was used in the composition of the pasted electrodes, which contained 10% of the conductive additive and 10% of the binder.

By classifying the works of [22–33], we can summarize that there are two primary ways to create electrodes for SCs. The first way is the direct formation of the electrochemically-active substances on the different current collectors. The advantage of the approach is the formation of the ready-to-use electrodes. The second way is the precipitation of the powders using physicochemical methods and the forming of the pasted electrodes based on the synthesized powder. The advantage of this approach is that the researcher has a much higher spectrum of methods for the synthesis. The second approach more often requires a binder and conductive additives such as carbon-based materials or metal powders. The addition of the extra components leads to a decrease in the electrochemically-active component content. In this case, the maximum possible achievable capacitance decreases.

In our opinion, the best strategy for developing SC materials is through the direct deposition of active materials onto the substrates. At the same time, the substrates must be constructed from highly conductive materials with a branch network, high porosity and roughness. Additionally, the substrates need to be of a relatively small thickness to prevent the current density inhomogeneity in the frontal and back sides of the electrodes. The latter occurs especially at high current densities and leads to a decrease in its efficiency. Using

the branched and slim substrates will allow for the depositing of the thin films of the active substances and, therefore, the cycling efficiency will increase. Moreover, the deposition onto the high-branched substrates will decrease the necessity for the co-deposition of the conductive additives.

From a large-scale production point of view, only relatively simple synthesis methods can be successful. These methods must not require specific reactants with high cost, multistage or complex procedures or steps with heating since this leads to a price rise in the final product.

This work proposed a facile formation method of the $Ni(OH)_2$ nanoflakes deposit decorated with nanosized $Co(OH)_2$ flower-like crystals. For this, the self-decomposition reaction of the nickel ammonia at room temperature was used with further improvements. The deposition was carried out on a nickel foam electrode. The required method does not need exotic reactants or heating and yields ready-to-use electrodes for hybrid supercapacitors. Based on the good electrochemical characteristics of the active material, the proposed method is suitable for the large-scale production of supercapacitors.

The main difference between the present and the relative works [34–36] is that the synthesis with the PVP presence was done at room temperature and the precipitated $Ni(OH)_2$ was modified by $Co(OH)_2$ in the second step.

2. Materials and Methods

2.1. Reactants

All the utilized chemicals were of the ACS reagent grade and used without any further purification. The metal precursors, including the nickel nitrate hexahydrate ($Ni(NO_3)_2{\cdot}6H_2O$, ≥98%), cobalt nitrate hexahydrate($Co(NO_3)_2{\cdot}6H_2O$, ≥98%), ammonium hydroxide (NH_4OH, 25%), potassium hydroxide (KOH) and polyvinylpyrrolidone (PVP, 29,000 a.m.u.), were purchased from Sigma Aldrich [37,38].

For the formation of the electrodes, the nickel foam (NF) substrates were used with the size 1 × 3.5 cm and with the following parameters: 99.99% purity, 1.6 mm thickness, 346 g/m^2 density and porosity ≥ 95%, 80–110 ppi.

2.2. Structural Characterization

The XRD analysis was carried out using a Bruker D8 ADVANCE diffractometer (Bruker, Billerica, MA, USA) equipped with an X-ray tube and a Co anode operating at 12 kW. All the measurements were performed using Bragg-Brentano geometry. The diffraction patterns were analyzed in the DIFFRAC.EVA v3.1 and TOPAS v4.2 softwares. All the diffraction patterns were measured in a wide scan range, from 20° to 110° with a step size of 0.025°. The time per step was 2 s.

2.3. Morphology and Composition

For the primary morphology estimation, an optical microscope with a digital camera (Hayear 16 MP) was used.

The electrodes were characterized using scanning electron microscopy (FEG250, FEI Company, Hillsboro, OR, USA) equipped with an energy-dispersive X-ray (EDX) spectroscope (XFlash 6-60, Bruker, Billerica, MA, USA).

The X-ray photoelectron spectroscopy (XPS—Omicron multiprobe system with hemispherical analyzer, Scienta Omicron GmbH, Taunusstein, Germany) was used to measure the chemical composition. The analysis was performed using monochromatic Al K-alpha X-rays (1486.6 eV). All the spectra were measured at ambient temperatures with a photoemission of 45 degrees from the surface. A low-energy electron gun was used for the charge neutralization to minimize the charging effects.

2.4. Electrochemical Characterization

For the electrochemical measurements, a Gamry 1010E potentiostat (Gamry Instruments, Warminster, PA, USA) was used. The platinum plate was employed as a counter

and Ag | AgCl in 3M KCl as the reference electrode. In all the experiments, a 1 M KOH solution was used as an electrolyte.

To calculate the specific capacity and capacitance from the discharge curves, the following equation was used:

$$C = I \cdot \tau / m \cdot (E_s - E_e), \quad (4)$$

$$Q = I \cdot \tau / m, \quad (5)$$

where C and Q are the specific capacitance and capacity in F/g and mA·h. I is current in A or mA for (4) and (5), respectively. T is the time of discharge in s or h for (4) and (5), respectively. m is the mass in g for the active substances ($Ni(OH)_2$, or $Ni(OH)_2$ plus $Co(OH)_2$). E_s and E_e are the potentials in V during the start and end of the discharge.

2.5. Formation of Electrodes

During the experiments, four types of electrodes were formed: $Ni(OH)_2$-pure, $Ni(OH)_2$-PVP, $Ni(OH)_2$-PVP-Co-elchem and $Ni(OH)_2$-PVP-Co-chem.

2.5.1. $Ni(OH)_2$-Pure Samples

Typically, obtaining the nickel ammonia solution was achieved via two steps—the formation of $Ni(OH)_2$ and its dissolution by NH_4OH. In the first stage, 3.14 g of $Ni(NO_3)_2 \cdot 6H_2O$ was dissolved in 20 mL of water and 2.46 g of KOH was dissolved in 40 mL of water. After that, the $Ni(NO_3)_2$ solution was added to the KOH at a continuous stirring rate of 770 rpm. The stirring was performed for 10 min. The obtained precipitate was filtered and rinsed once with water from the KNO_3 solution on a paper filter. The last stage was the dissolution of the nickel hydroxide using 40 mL of NH_4OH. As a result, a blue transparent solution of nickel ammonia complex was prepared. To form the $Ni(OH)_2$-pure samples, four pieces of NF remained in a 15 mL nickel ammonia complex for 24 h. After the precipitation, the electrodes were rinsed in water and dried in the air for 24 h. The initial and final NF mass was controlled for all the samples on the analytical balance with an accuracy of ± 0.00001 g.

2.5.2. $Ni(OH)_2$-PVP Samples

The $Ni(OH)_2$-PVP samples were obtained in the same way as the $Ni(OH)_2$-pure samples with slight modifications. First, 0.17 g of PVP was dissolved in 5 mL of water. After that, 2 mL of PVP solution was added to 15 mL of the nickel ammonia complex. The formation of the $Ni(OH)_2$-PVP samples was carried out by leaving four pieces of NF in 17 mL of the resulting solution for 48 h. The electrodes were rinsed, dried and weighed as described above.

2.5.3. $Ni(OH)_2$-PVP-Co-Elchem Samples

The $Ni(OH)_2$-PVP-Co-elchem samples were obtained through the modification of the $Ni(OH)_2$-PVP samples. After the $Ni(OH)_2$ formed on the NF surface, the samples were modified by the electrochemical deposition of cobalt hydroxide at a constant current from 0.1 M of the $Co(NO_3)_2$ solution. The electrodeposition was achieved by applying a constant cathodic current for 1 h. A specific current was calculated based on the $Ni(OH)_2$ mass in order to deposit 20% cobalt hydroxide by mass. For example, if the $Ni(OH)_2$ mass was 20 mg, the applied current was 2.31 mA (i.e., j = 0.116 mA/mg($Ni(OH)_2$)). After the electrodeposition, the electrodes were rinsed, dried and weighed as described above.

2.5.4. $Ni(OH)_2$-PVP-Co-Chem Samples

The $Ni(OH)_2$-PVP-Co-chem samples were obtained through the modification of the $Ni(OH)_2$-PVP samples. After the $Ni(OH)_2$ formed on the NF surface, the samples were modified by soaking it in a 1 M $Co(NO_3)_2$ solution. The excess $Co(NO_3)_2$ solution was removed by applying the filter paper to the surface of the wet electrode. After that, the electrodes were dried for 24 h in the air. In the next step, the weighted electrodes were

immersed in the 1 M KOH solution for 1 h. The electrodes were rinsed, dried and weighed as described above.

3. Results

The overall scheme of the experiments is shown in Figure 1. The addition of PVP was used on the basis of its surfactant properties [39,40] and our previous works were dedicated to the $Ni(OH)_2$ electrochromic films [41,42]. It was proposed that the addition of PVP would affect the morphology of the deposits and (or) the composition through the $Ni(OH)_2$–PVP composite formation. This could improve the adhesion and mechanical properties of the formed films and thereby their electrochemical properties. It has to be underlined that the adhesion to a substrate and its certain flexibility play a critical role in the performance of the nickel hydroxide-based materials.

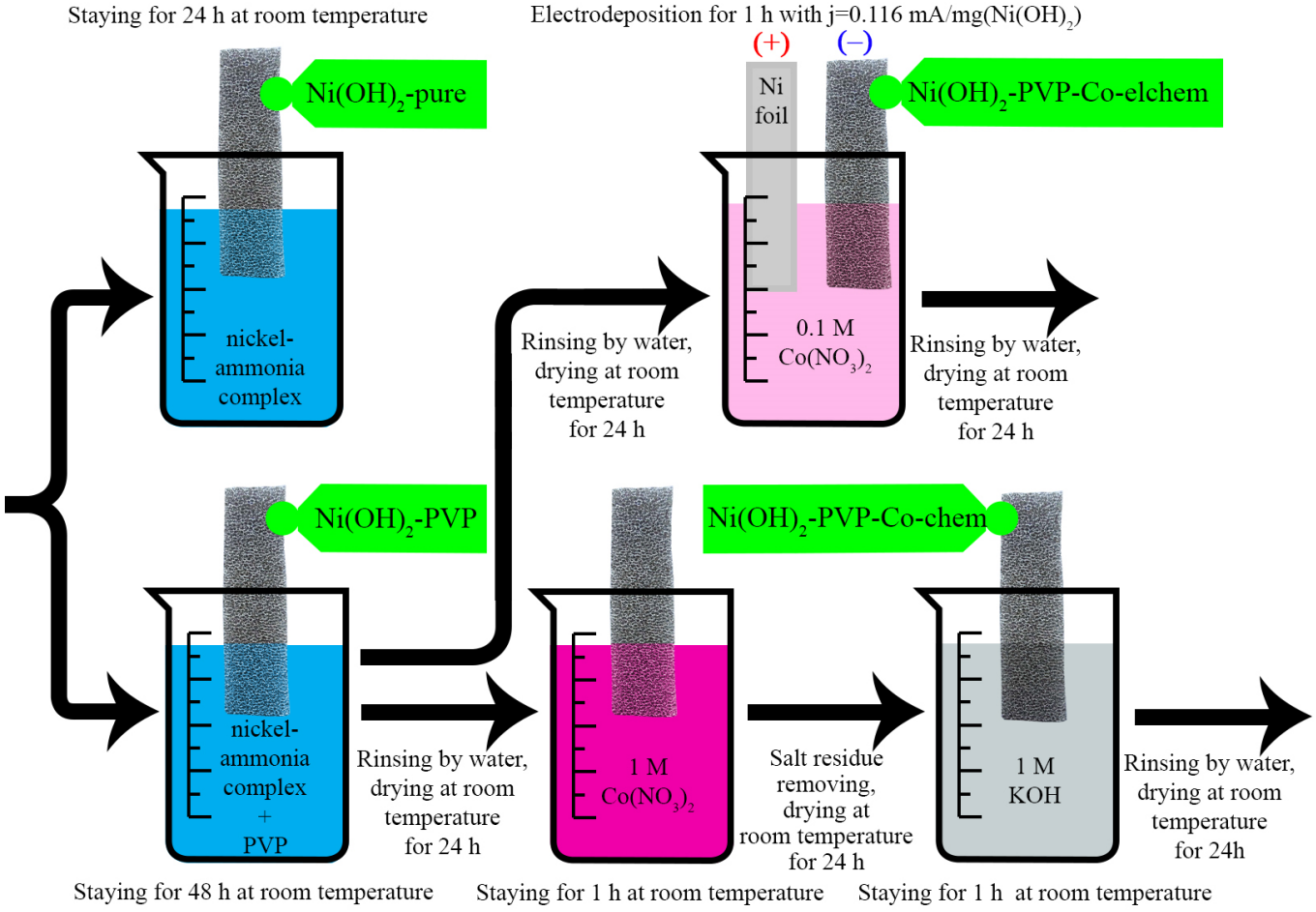

Figure 1. The general simplified scheme of the electrode formation. Detailed information about formation conditions is presented in Section 2.5.

During a charge on a nickel electrode, oxygen evolution occurred and was considered a harmful process [43,44]. The oxygen evolution decreased the charge efficiency and broke the active material–substrate contact. In addition, the oxygen evolution led to the shedding of the active material. Another performance problem with the nickel materials was the possible change in the electrode sizes during the cycling process [45,46]. The reason for this was the different crystal lattice sizes of the certain charged and discharged forms. In this case, the PVP addition increased the electrochemical properties of the electrode by eliminating the listed reasons.

The next step was improving the deposits' electrochemical properties via the additional precipitation of cobalt hydroxide. It was essential to deposit the $Co(OH)_2$ after the $Ni(OH)_2$

formation. The effect was better if the cobalt hydroxide covered the nickel hydroxide surface [47]. The cobalt hydroxide enhancing mechanism differed from work to work. In [48], the efficiency increase was explained by the higher oxygen evolution overpotential with a simultaneous decrease in the redox potential. Other authors showed the formation of a highly conductive mixed oxyhydroxide $Co^{4+}{}_xCo^{3+}{}_{1-x}OOH_{1-x}$ that enhanced the overall conductivity [49].

For the $Co(OH)_2$ formation, two different methods were chosen. The first method was electrodeposition from a relatively diluted cobalt nitrate solution in order to obtain 20% of the mass from the nickel hydroxide (6) and (7):

$$2H_2O + 2e^- \rightarrow H_2 + 2OH^-, \quad (6)$$

$$Co^{2+} + 2OH^- \rightarrow Co(OH)_2\downarrow. \quad (7)$$

The second method was conducted by means of electrode soaking with concentrated $Co(NO_3)_2$, drying it and immersing it in KOH. In this case, $Co(OH)_2$ was formed in a single reaction (3):

$$Co(NO_3)_2 + 2KOH \rightarrow Co(OH)_2\downarrow + 2KNO_3. \quad (8)$$

The X-ray diffractograms for the electrodes with the deposits are presented in Figure 2. In all the cases, the peaks for the metallic nickel and β-$Ni(OH)_2$ were identified. The sizes of the crystallites were several tens of nm with lattice parameters of a = 3.1273 Å, c = 4.6439 Å. The $Co(OH)_2$ reflects were not detected. This fact can be explained by a lower quantity of cobalt hydroxide.

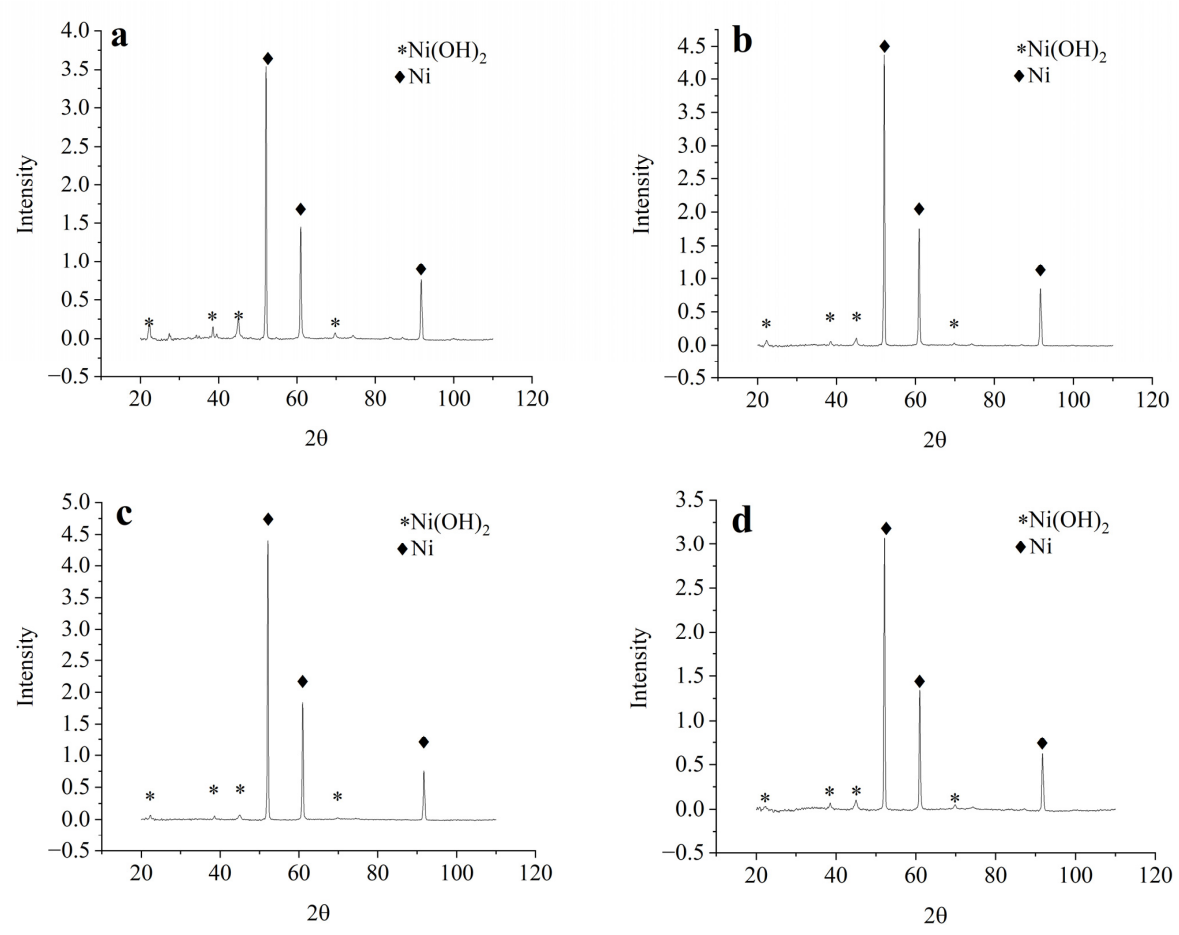

Figure 2. X-ray diffractograms recorded for formed electrodes: (**a**) $Ni(OH)_2$-pure; (**b**) $Ni(OH)_2$-PVP; (**c**) $Ni(OH)_2$-PVP-Co-elchem; (**d**) $Ni(OH)_2$-PVP-Co-chem.

For the primary estimation of morphology, the images for the $Ni(OH)_2$-pure samples before and after cycling were photographed. It has to be noted that nickel hydroxide has a light green color [50] and the oxidized NiOOH phase has a black color [51].

Analyzing Figure 3a allows us to conclude that the surface of the $Ni(OH)_2$-pure sample was covered by highly branched $Ni(OH)_2$ particles. A more interesting picture is seen for the cycled electrode—Figure 3b. The hydroxide that covers the NF turned black. At the same time, a few particles that had a highly branched morphology were still green. This fact can be explained by the high resistance of particle roots and the long route of the current. More likely, the particle roots had a low cross-sectional area (S) and according to Equation (3), the resistance (R) was high enough to cause a very high IR-drop as well. A high IR-drop value will lead to an inability to conduct the electrochemical process in remote parts of the branched particles.

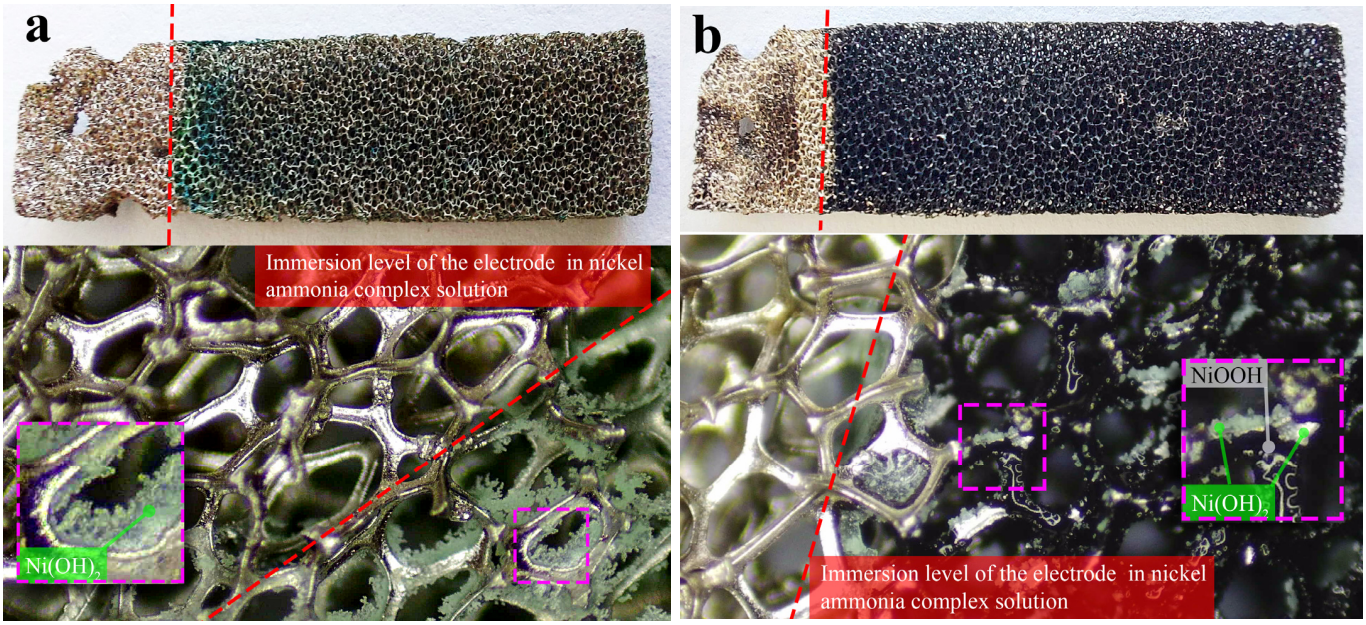

Figure 3. Comparison of the freshly-synthesized and cycled electrodes by means of optical microscopy for the $Ni(OH)_2$-pure sample: (**a**) before the charge–discharge experiments; (**b**) after the charge–discharge experiments.

The morphology at a low magnification of the electrodes is shown in Figure 4. It is clearly seen that all the electrodes formed without PVP do not have branched particles. On the contrary, Figure 4a clearly demonstrates that the absence of PVP in the solution leads to the formation of highly branched particles on an NF surface. These particles resemble grey fur on the surface.

At higher magnifications, the surfaces of all the electrodes consist of flakes with nanosized thickness—Figure 5a–d. The electrode that was chemically activated with cobalt hydroxide differs in comparison with the other samples. Except for the nanoflakes, the surface contains flower-like crystals with nanosized thickness—Figure 5d–f. In Figure 5e, the flower-like crystals are highlighted by a dotted line.

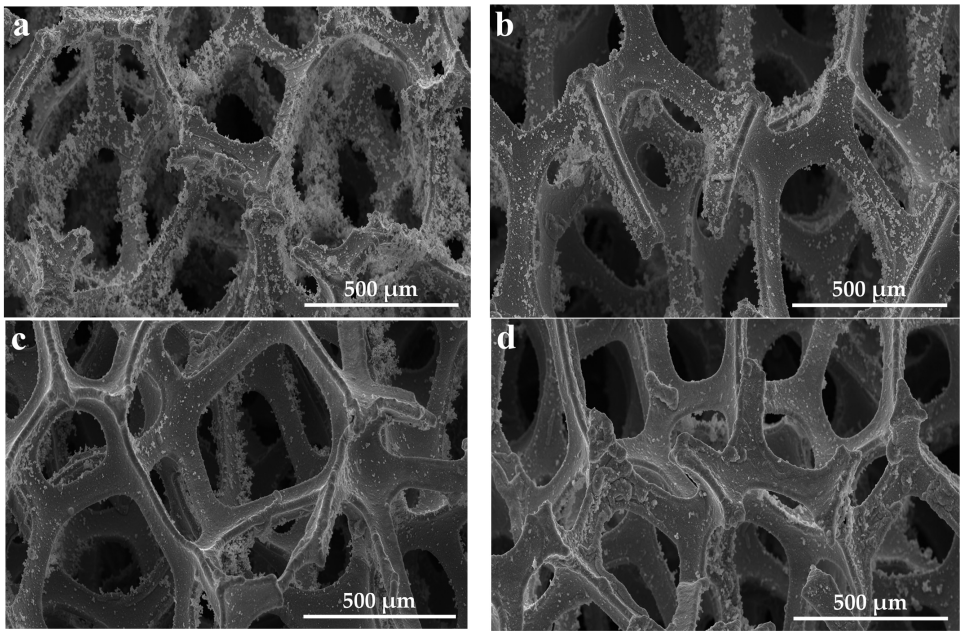

Figure 4. SEM images of the samples: (**a**) $Ni(OH)_2$-pure; (**b**) $Ni(OH)_2$-PVP; (**c**) $Ni(OH)_2$-PVP-Co-elchem; (**d**) $Ni(OH)_2$-PVP-Co-chem.

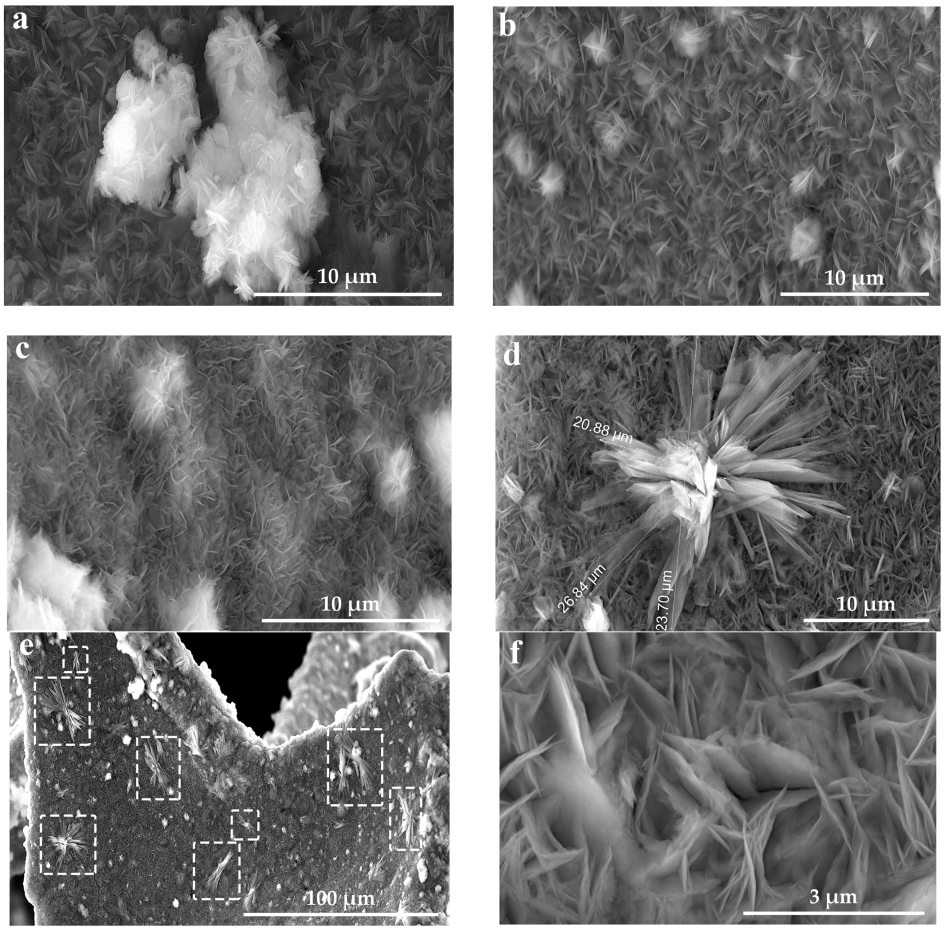

Figure 5. SEM images of the samples: (**a**) $Ni(OH)_2$-pure; (**b**) $Ni(OH)_2$-PVP; (**c**) $Ni(OH)_2$-PVP-Co-elchem; (**d**–**f**) $Ni(OH)_2$-PVP-Co-chem.

The specific surface area of the active substances is an important value for supercapacitor performance [52]. For similar deposition methods, this value is approximately equal to 10^2 m^2/g [3]. Nevertheless, a comparison of the SEM images indirectly proves that the specific surface area is not affected by the synthesis modifications used.

To determine the cobalt distribution on the NF surface, the maps of the elements were defined—Figure 6. Two differences between the activation methods were detected. For the electrochemically activated sample ($Ni(OH)_2$-PVP-Co-elchem), the distribution of cobalt was relatively uniform. This fact means that the nickel hydroxide film had a high porosity and allowed the electrochemical reaction (6). coupled with the chemical reaction (7). On the other hand, the chemical activation leads to a non-uniform cobalt distribution and flower-like crystals consist of a cobalt hydroxide formed with the reaction (8).

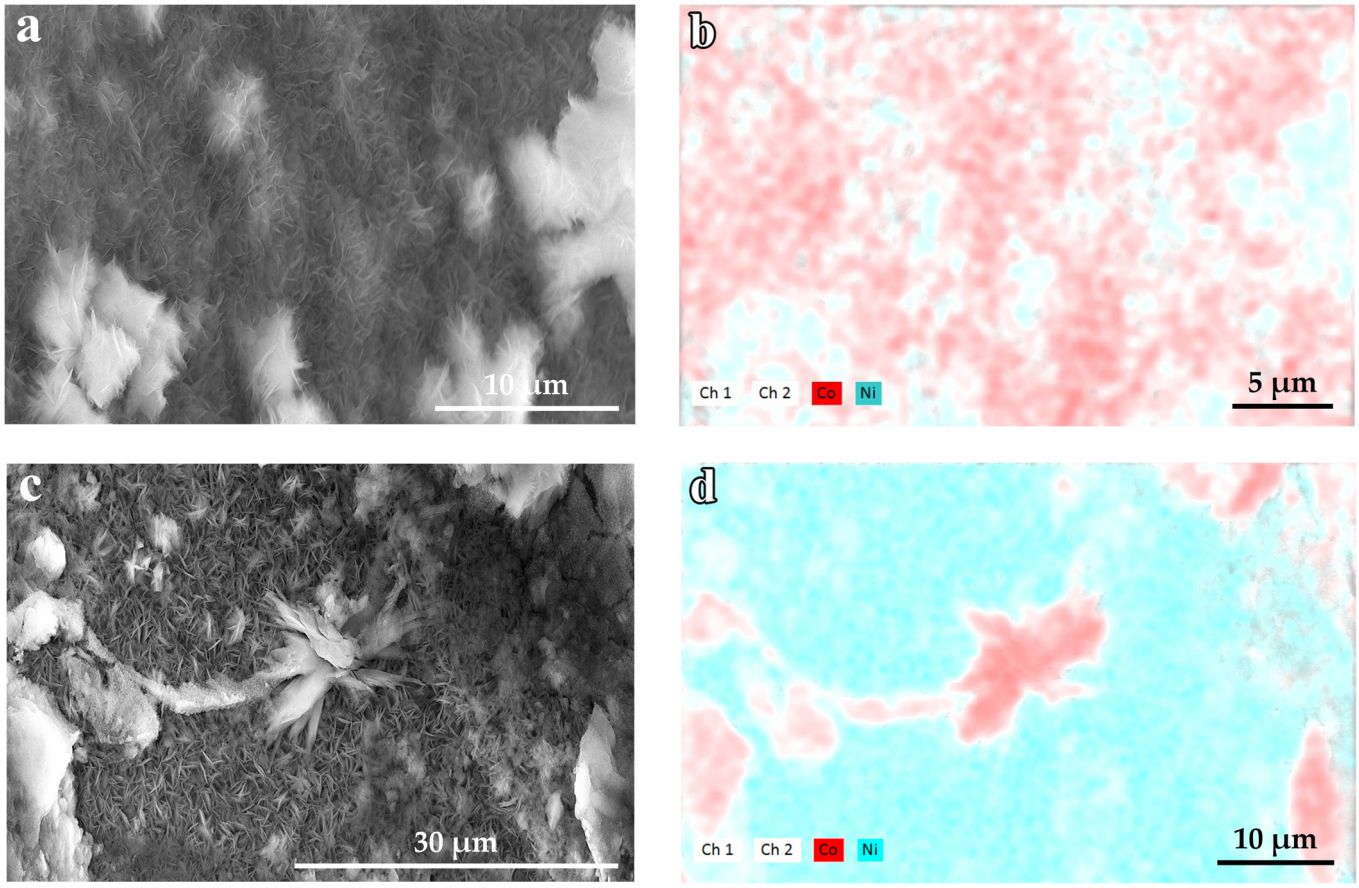

Figure 6. SEM images and the corresponding element distribution of the samples: (**a**,**b**) $Ni(OH)_2$-PVP-Co-elchem; (**c**,**d**) $Ni(OH)_2$-PVP-Co-chem (flower-like crystal in the center).

For analyzing the composition of the films formed on the substrates, an XPS analysis was carried out—Figure 7. Depending on the formation method, the electrode composition consisted of potassium, oxygen, carbon and cobalt. The electrodes activated with cobalt hydroxide contained cobalt. It was the most interesting to analyze the changes in the carbon content. In the $Ni(OH)_2$-pure sample, the carbon percentage was estimated at 27%. After using PVP during the electrode formation, the carbon percentage rose to almost 40%. However, in the case of further cobalt activation by two methods, the carbon content decreased to 12.1 and 22.6% for electrochemical and chemical activation, respectively. This can be explained by a chemicalism of the processes. It is well-known that potassium alkaline intensively absorbs carbon dioxide, according to Equation (9):

$$2KOH + CO_2 \rightarrow K_2CO_3 + H_2O. \quad (9)$$

As far as the obtaining procedure of the nickel ammonia complex requires KOH solution, K_2CO_3 was in the resulting solution. This caused the initial concentration of carbon that is captured from the deposited solution. When the PVP solution was added, the carbon concentration grew. This was explained by either the $Ni(OH)_2$-PVP composite formation or the PVP absorption on the surface. It has to be noted that both methods of cobalt activation contain intermediate rinsing stages. In the case of the composite formation, the PVP molecules were in the composite structure and rinsing did not affect PVP quantity. If PVP acts only as a surfactant, further rinsing will decrease the carbon content. Based on these considerations and the decrease in the carbon content after the activations, it can be assumed that PVP acts only as the surfactant and prevents the formation of highly branched particles.

To define the electrochemical differences for the formed electrodes, the cyclic voltammetry curves (CV curves) were recorded in a 1 M KOH solution. The CV curves are presented in Figure 8. The comparison of the CVs showed sharp differences between the electrochemical behavior of the samples. The form, position and specific currents of the peaks differed for the electrodes. The electrodes with cobalt activation demonstrated higher specific currents of the peaks in comparison to the electrodes without activation. The $Ni(OH)_2$-pure sample had lower peaks compared to the electrode formed with PVP-$Ni(OH)_2$-PVP.

For a semi-quantitative comparison of the transport properties of the formed electrodes, the dependencies between the cathodic current peaks versus the root of the sweep rates were plotted—Figure 9. Many researchers used these dependencies and the Randles–Sevcik equation for the diffusion of the proton estimation—Equation (10) [53–56].

$$I = 2.69 \cdot 10^5 \cdot n^{3/2} \cdot S \cdot D^{1/2} \cdot C_0 \cdot \upsilon^{1/2}, \quad (10)$$

where n is the electron number of the reaction (1 for $Ni(OH)_2$, Equation (1)), S is the surface area of the electrode, D is the diffusion coefficient of the protons (Equation (1)), υ is the sweep rate and C_0 is the initial concentration of the diffused ions H^+.

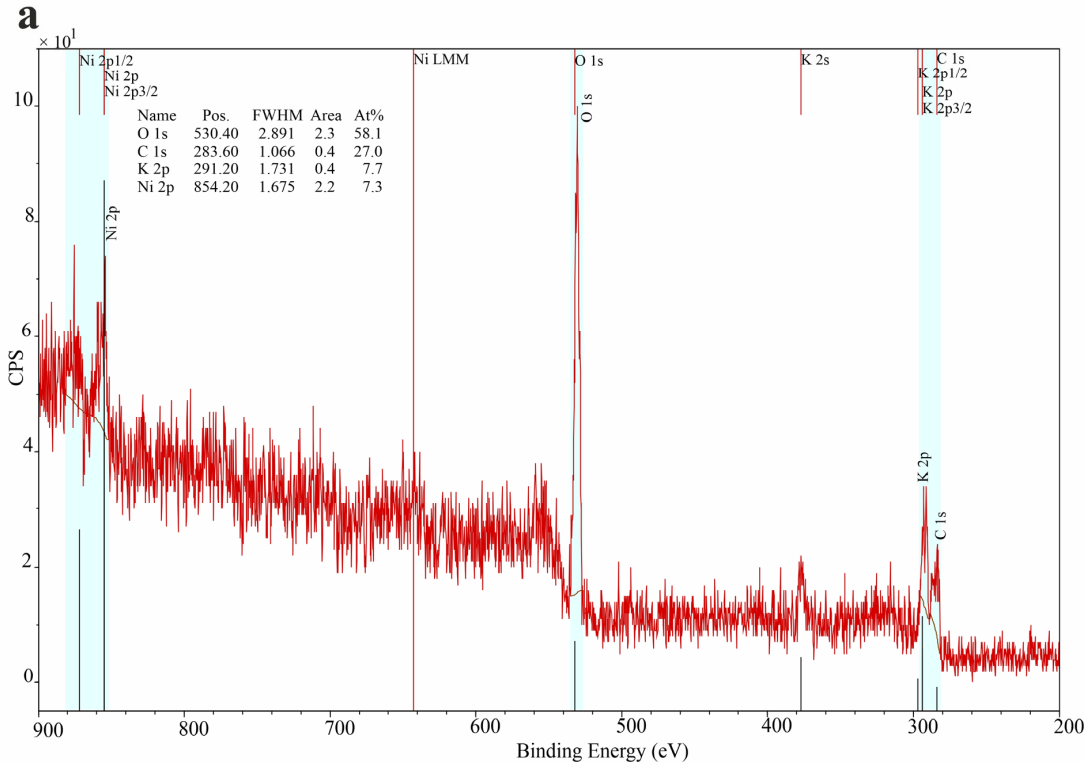

Figure 7. *Cont.*

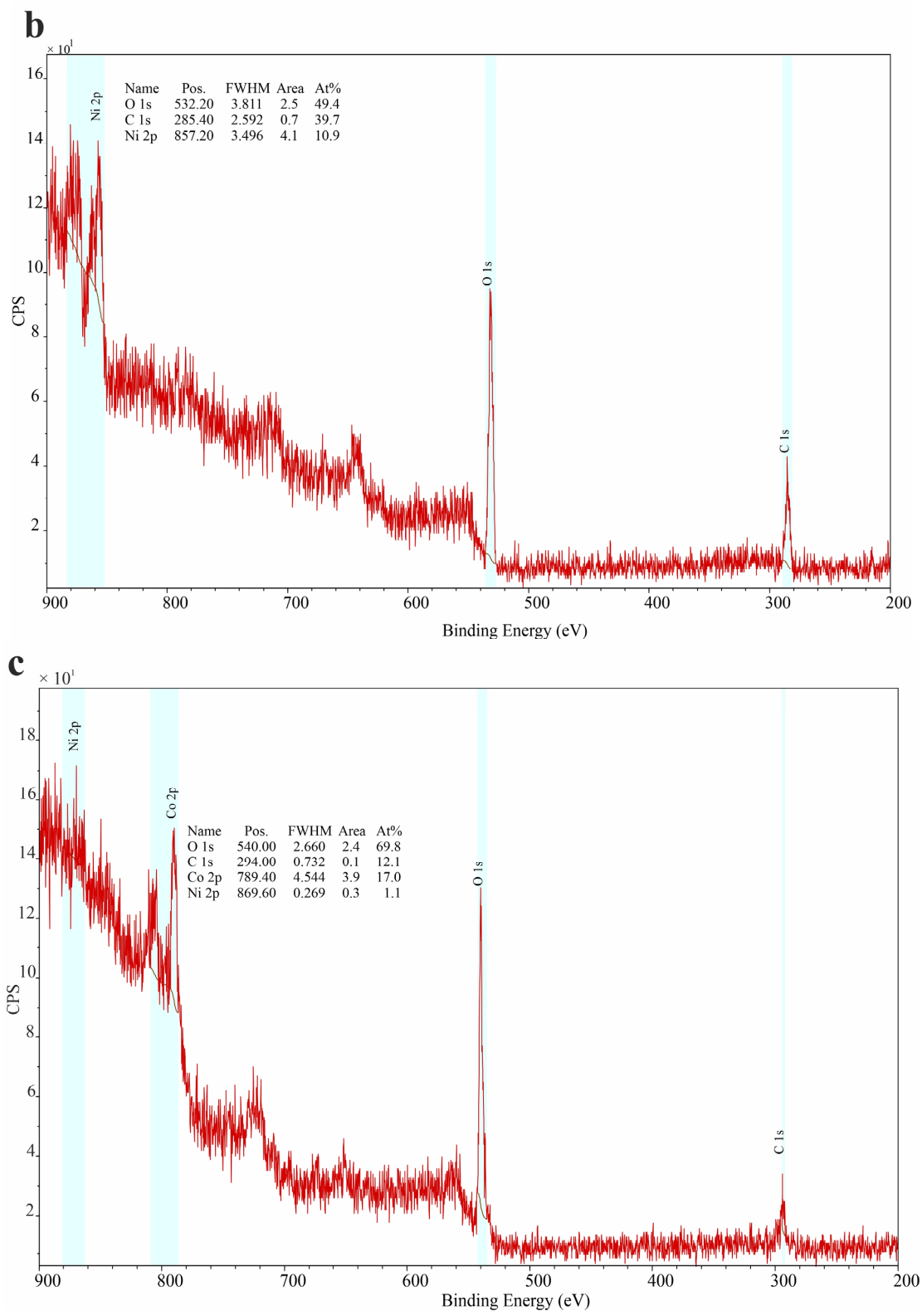

Figure 7. *Cont.*

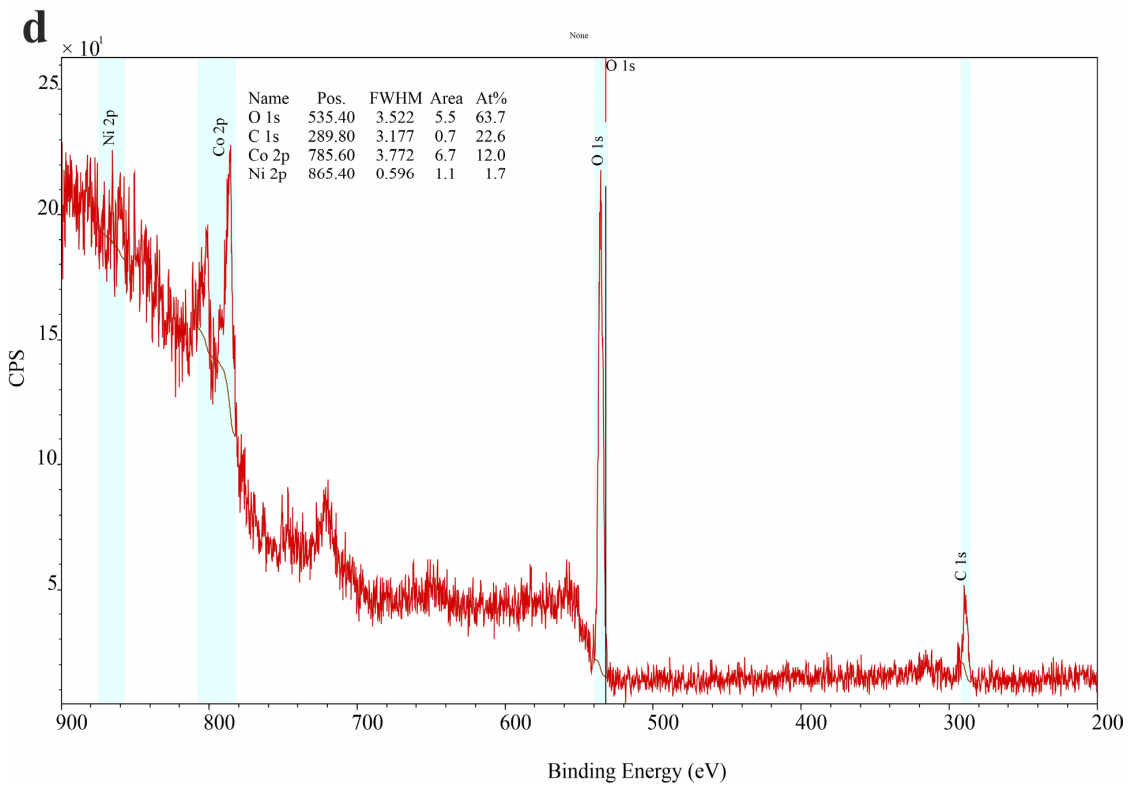

Figure 7. EDX spectra and the compositions for the samples: (**a**) $Ni(OH)_2$-pure; (**b**) $Ni(OH)_2$-PVP; (**c**) $Ni(OH)_2$-PVP-Co-elchem; (**d**) $Ni(OH)_2$-PVP-Co-chem.

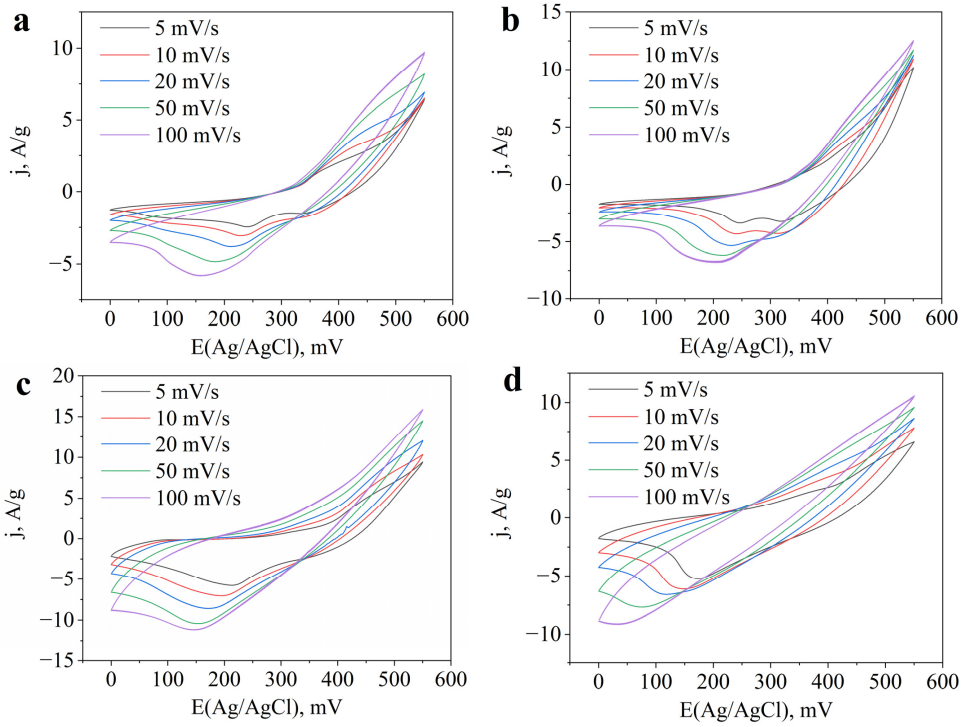

Figure 8. Cyclic voltammetry curves at the different sweep rates for (**a**) $Ni(OH)_2$-pure; (**b**) $Ni(OH)_2$-PVP; (**c**) $Ni(OH)_2$-PVP-Co-elchem; (**d**) $Ni(OH)_2$-PVP-Co-chem.

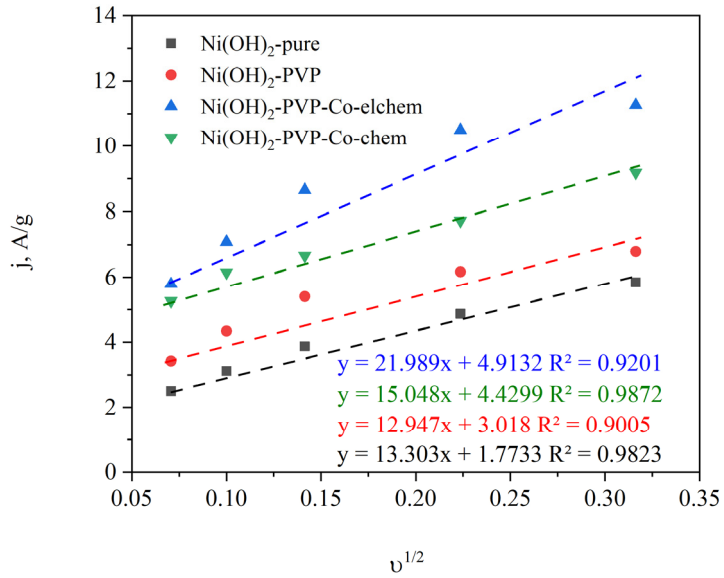

Figure 9. Dependence between the specific cathodic currents of the peaks and the sweep rate roots.

Equation (10) can be rewritten as follows:

$$S \cdot D^{1/2} = \frac{I}{2.69 \cdot 10^5 \cdot n^{3/2} \cdot C_0 \cdot \upsilon^{1/2}} = \frac{1}{2.69 \cdot 10^5 \cdot n^{3/2} \cdot C_0} \cdot \frac{I}{\upsilon^{1/2}} = a \cdot x, \quad (11)$$

where a is the constant for the current material because it consists of constants $a = \frac{1}{2.69 \cdot 10^5 \cdot n^{3/2} \cdot C_0}$ and x is a slope factor defined from j-$\upsilon^{1/2}$ curves $x = \frac{I}{\upsilon^{1/2}}$.

Therefore, it is possible to compare the transport characteristics of the electrodes by comparing the appropriate slope factors. A comparison of the slope factors showed that the $Ni(OH)_2$-PVP-Co-elchem sample had the highest value. The electrodes obtained with and without PVP had almost similar slope factors of 12.947 and 13.303. At the same time, the chemically activated electrode had a moderate slope factor of 15.048. Therefore, the electrochemically activated electrode had higher transport characteristics.

It should be noted that researchers need to use such comparisons with caution. This is due to several reasons. First, the Randles–Sevcik equation was formulated for diffusion in a liquid solution, not for materials with solid-state reactions. Moreover, it does not account for the active material conductivity and its change. In addition, the materials with a high specific surface area had an additional part of current peaks caused by a double-layer charge and discharge [57].

The discharge curves for the samples are shown in Figure 10. The analysis of the presented curves revealed that the first step of the nickel hydroxide formation and the second step of the activation by cobalt affected the parameter curves—shapes, potentials and discharge times. The highest times of discharge were detected for the $Ni(OH)_2$-PVP-Co-chem sample. Based on the discharge curves, the dependencies between the specific capacitance and capacity and the specific current density were calculated—Figure 11.

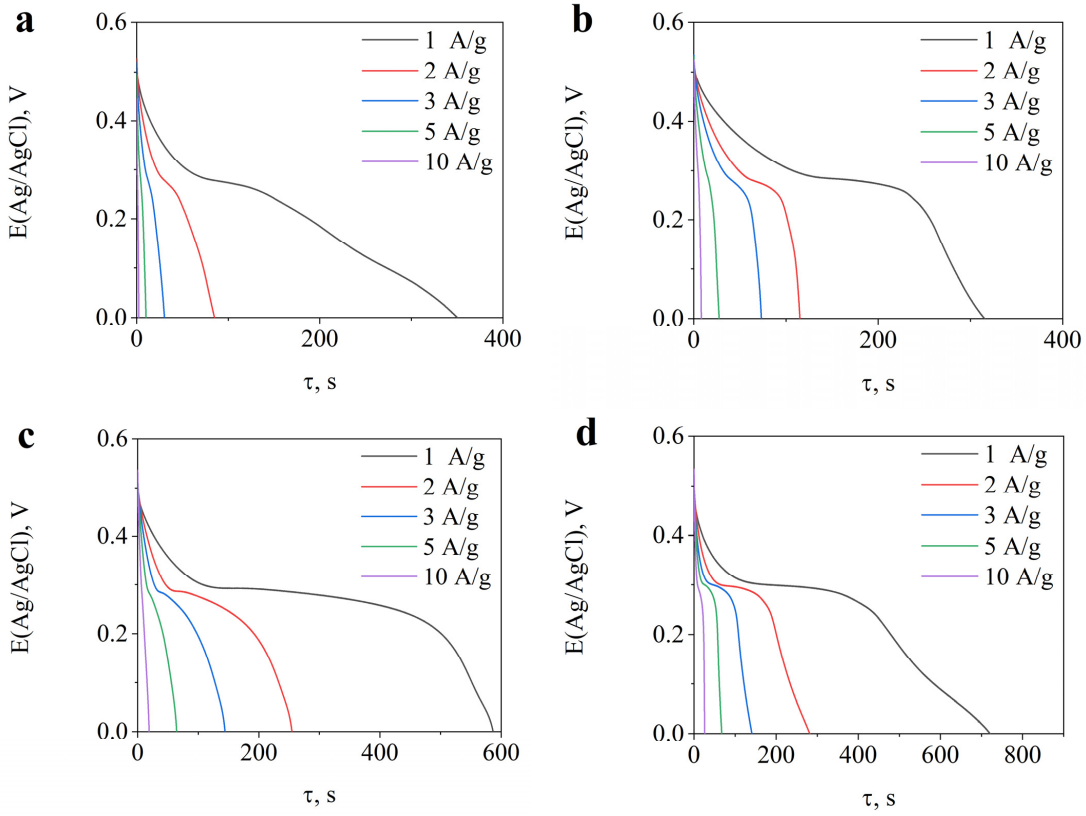

Figure 10. Discharge curves at the different current densities for: (**a**) $Ni(OH)_2$-pure; (**b**) $Ni(OH)_2$-PVP; (**c**) $Ni(OH)_2$-PVP-Co-elchem; (**d**) $Ni(OH)_2$-PVP-Co-chem.

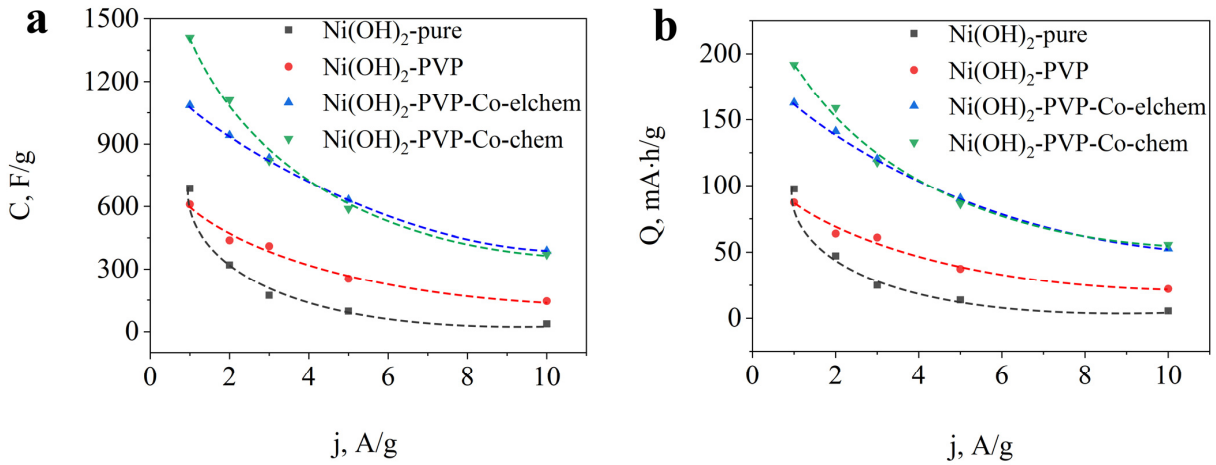

Figure 11. Specific capacitance (**a**) and capacity (**b**) and the specific current density dependencies for electrodes mass loadings were $Ni(OH)_2$-pure—18.7 mg; $Ni(OH)_2$-PVP—19.8 mg; $Ni(OH)_2$-PVP-Co-elchem—17.3 mg; $Ni(OH)_2$-PVP-Co-chem—13.3 mg.

It was found that the capacitance of the sample deposited with PVP was higher at high current densities. but in relatively low current densities. the capacitance was almost the same—Figure 11a,b. This fact is explained in Figure 12. The surface of the electrode formed without PVP contained branched particles that were attached to the surface —Figure 12a. Each particle was connected with the surface of the electrode with a root that had a low transitional resistance $R_{F\text{-}P}$. The $R_{F\text{-}P}$ resistance was low due to the low cross-section area and the inhomogeneity of the root which consisted of nanoflakes. In this case, the IR

drop at low currents was low as well and all the particles were electrochemically-active. At higher currents, the IR drop in the roots was so high that the potential in the surface of the particles was much lower, which did not allow for the discharge process to begin. Therefore, the formation of the suppressing of the highly branched particles was one of the essential keys for supercapacitor materials development. The cobalt activation by both methods led to higher capacitances, but the chemically-activated nickel hydroxide had better performance at lower current densities. It was shown earlier that the chemically activated $Ni(OH)_2$-PVP-Co-chem sample contained flower-like particles—Figure 5d,e. In this case, we assumed that the cobalt hydroxide flower-like particles worked well at low current densities for the same reason as the PVP use.

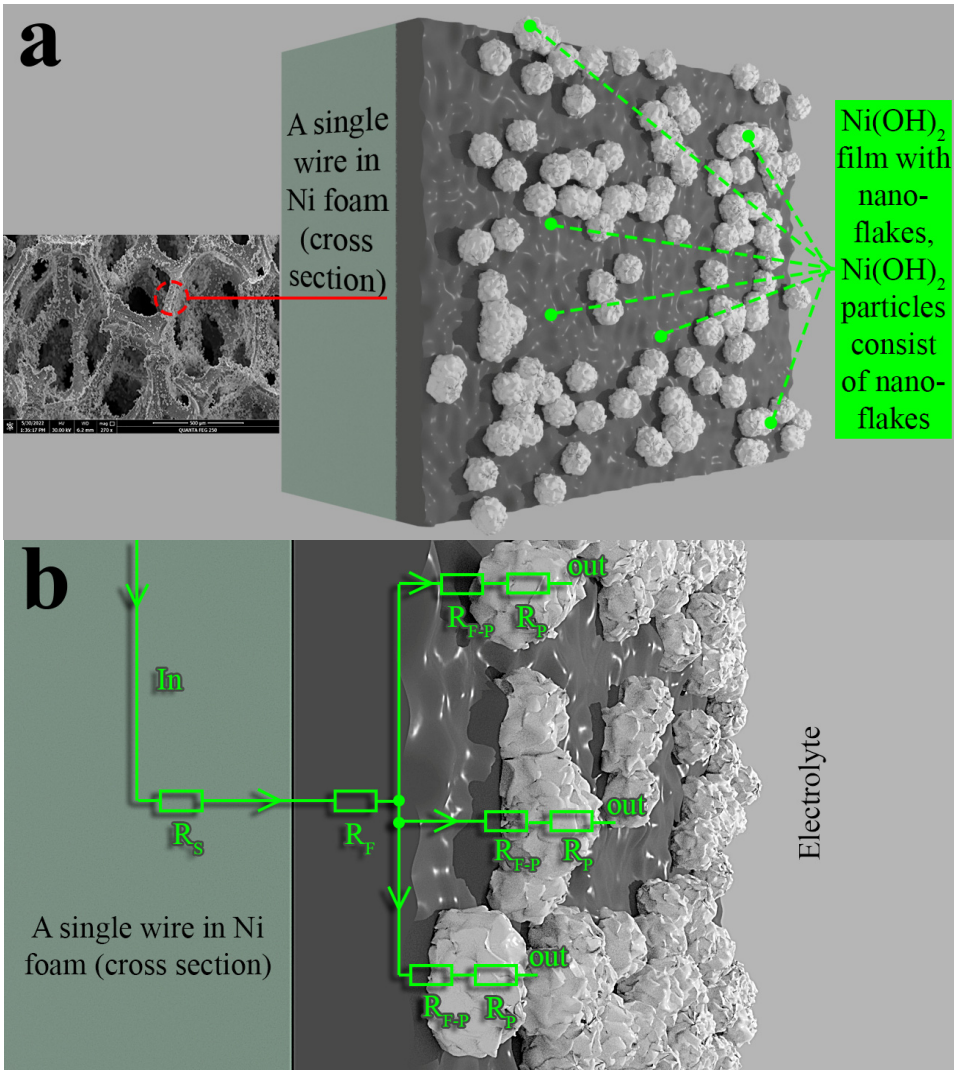

Figure 12. Generalized equivalent scheme of the electrode resistive components. 3D generated image of $Ni(OH)_2$-pure electrode: (**a**) general view and (**b**) current flows through the electrode where R_S—substrate resistance, R_F—film resistance, $R_{F\text{-}P}$—transitional resistance from film to particle, R_P—resistance of a single particle.

The possibility of the synthesis method implementation of SC active substances for large-scale production was defined by the method's prime cost. The prime cost was affected by the number and cost of the used reactants, the complexity of the synthesis method and the heating requirement. The absence of heating during synthesis can lower the prime cost. Moreover, the formation of the ready-to-use electrodes was much better due to the absence of an additional stage in forming the electrodes. It should be noted

that additional substances are usually used at the formation stage—conductive additives, activators, additives against clumping, binders, etc. However, these compounds can increase production costs as well.

To compare the obtained capacitances, the number of the used reactants and the heating requirement for the proposed and other synthesis methods (Table 1) were formed based on the literature. The order of the table is by descending capacitances.

Table 1. Comparison of the synthesis methods in the framework of their complexity and primary cost. Capacitances, the number of the used reactants and the heating requirements for the proposed and other synthesis methods are represented.

Sample	Specific Capacitance, Electrolyte	Number of Used Reagents [1]	Heating Requirement (Conditions)	Direct Formation on the Substrate	Ref.
$Ni(OH)_2$ coated carbon NP mediated hybrid three-dimensional graphene	4667 F g^{-1} at 2 A g^{-1} in 1 M KOH	6	Yes (1000 °C)	Yes	[30]
$NiMnO_3/Ni(OH)_2$	2454 F g^{-1} at 1 A g^{-1} in 2 M KOH	9	Yes (80 °C)	Yes	[27]
Hollow Ni-Co LDH nanocages	2369 F g^{-1} at 0.5 A g^{-1} in 2 M KOH	4	Yes (90 and 60 °C)	No	[31]
$Ni(OH)_2/ZnO$	2265 F g^{-1} at 1 A/g in 6M KOH	4	Yes (60 °C)	Yes	[26]
$Ni/SnS_2@Ni(OH)_2$-CC	2090 F g^{-1} at 1 A g^{-1} in 2 M KOH	6	Yes (160, 100, 60 °C)	Yes	[24]
La decorated $Ni(OH)_2$ nanosheets	1510.7 F g^{-1} at 1 A g^{-1}	7	Yes (70 °C)	No	[33]
This work	**1408 F g^{-1} at 1 A g^{-1} (191.7 mA·h·g^{-1}) in 1 M KOH**	**4**	**No**	**Yes**	**-**
Hierarchical hollow nanocages of Ni-Co LDH	1198 F g^{-1} at 1 A g^{-1} in 2 M KOH	8	Yes (60 °C)	No	[58]
Co_3O_4 embedded α-Co/$Ni(OH)_2$ hollow nanocages	1000 F g^{-1} at 1 A g^{-1}	-	-	No	[59]
Ni–Co LDH/STSC	992.2 F g^{-1} at 1 A g^{-1} in 1 M KOH	6	Yes (600, 800, 100 °C)	No	[60]
NiNF@TBC	945 F g^{-1} at 1 A g^{-1} in 1 M Na_2SO_4	4	Yes (800, 600, 160, 110, 80, 70 °C)	No	[23]
CoNi-DH/NHCS	578 C g^{-1} (160 mA·h·g^{-1}) at 1 A g^{-1} in 1 M KOH	14	Yes (50, 800, 80 °C)	No	[22]
Nickel oxide-porous carbon composite	811 F g^{-1} at 1 A g^{-1} in 6 M KOH	2	Yes (700, 80 °C)	No	[61]
Hierarchical Co_3O_4-NiO/graphene foam	766 F g^{-1} at 1 A g^{-1} in 2 M KOH	5	Yes (60, 350 °C)	Yes	[62]
Ni-Co LDH nanosheets with RGO	642 F g^{-1} at 10 A g^{-1} in 1 M KOH	4	Yes (180, 80, 550 °C)	Yes	[63]
Micro-nano assembled Mn_2O_3/NiO composite	566.21 F g^{-1} at 0.5 A g^{-1} in 1 M KOH	4	Yes (120 °C)	No	[64]
$Ni(OH)_2$/g-C_3N_4	463 F g^{-1} at 1 A g^{-1} in 1 M KOH	3	No	Yes	[32]
NiO@SW-CFs	356 F g^{-1} at 2 A g^{-1} in 1 M KOH	5	Yes (100, 800 °C)	No	[65]
NiO synthesized by solution combustion method	174.7 C/g at 10 A/g (58.9 mA·h·g^{-1})	2	Yes (50, 100, 300 °C)	No	[66]

[1]—water is not counted; multiple uses of the same reagent are counted as the use of one reagent.

The comparison of the methods and capacities revealed that the majority of the methods used one or several heating operations during the formation of the active substances or masses. The formation of the ready-to-use electrodes was less common among the methods. In addition, many methods used more than four reactants and some of them had a high price.

In comparison to the other methods [22–24,26,27,30–33,58–66], the proposed direct formation of a ready-to-use electrode was easy to implement and did not require exotic components and high price reagents. It also did not require heating. Simultaneously with the aforementioned, the resulting electrodes had relatively high capacitance and high mass loading [67].

4. Conclusions

It was found that the best way to form a ready-to-use electrode was through the decomposition of the nickel ammonia complex in the presence of PVP with subsequent chemical activation. The resulting electrode had a capacitance of 1408 F g^{-1} at 1.0 A g^{-1}.

It was shown that the presence of PVP in the nickel ammonia complex suppressed the formation of the highly branched particles on the electrode surface. At the same time, it was demonstrated that the formation suppression of the highly branched particles increased the electrode's specific capacitance at high specific charge–discharge currents. The mechanism of the effect was explained by an increase in the IR drop in the roots of the highly branched particles.

In addition, it was found that the chemical and electrochemical activation by cobalt hydroxide led to a uniform and nonuniform formation of $Co(OH)_2$ particles, respectively.

Author Contributions: Conceptualization, V.K. (Valerii Kotok), P.O. and M.M.; methodology, V.K. (Valerii Kotok), P.O., M.M. and V.K. (Vadym Kovalenko); validation, V.K. (Valerii Kotok), P.O. and M.M.; formal analysis, V.K. (Valerii Kotok) and P.O.; investigation, V.K. (Valerii Kotok), P.O., M.M., M.S., P.N. and M.G.; resources M.M.; data curation, V.K. (Valerii Kotok); writing—original draft preparation, V.K. (Valerii Kotok); writing—review and editing, V.K. (Valerii Kotok), P.O. and V.K. (Vadym Kovalenko); visualization, V.K. (Valerii Kotok) and P.O.; supervision, M.M. and K.S.; project administration, P.O. and M.M.; funding acquisition, M.M., V.K. (Valerii Kotok) and K.S. All authors have read and agreed to the published version of the manuscript.

Funding: This research was funded by National Scholarship Program of the Slovak Republic with the assistance of the Slovak Academic Information Agency (S.A.I.A, n.o.); by the Ministry of Education, Science, Research and Sport of Slovakia under grant VEGA 1/0529/20; and by the Slovak Research and Development Agency under grants APVV-21-0278, APVV-20-0220, and APVV-21-0231.

Conflicts of Interest: The authors declare no conflict of interest.

References

1. Cui, Z.; Kang, L.; Li, L.; Wang, L.; Wang, K. A hybrid neural network model with improved input for state of charge estimation of lithium-ion battery at low temperatures. *Renew. Energy* **2022**, *198*, 1328–1340. [CrossRef]
2. Li, D.; Yang, D.; Li, L.; Wang, L.; Wang, K. Electrochemical impedance spectroscopy based on the state of health estimation for lithium-ion batteries. *Energies* **2022**, *15*, 6665. [CrossRef]
3. Kovalenko, V.; Kotok, V. Definition of effectiveness of β-$Ni(OH)_2$ application in the alkaline secondary cells and hybrid supercapacitors. *East.-Eur. J. Enterp. Technol.* **2017**, *5*, 17–22. [CrossRef]
4. Djafri, D.; Henni, A.; Zerrouki, D. Electrochemical synthesis of highly stable and rapid switching electrochromic $Ni(OH)_2$ nanoflake array films as low-cost method. *Mater. Chem. Phys.* **2022**, *279*, 125704. [CrossRef]
5. Wang, W.; Li, Z.; Yu, Z.; Su, G. The stabilization of $Ni(OH)_2$ by In_2O_3 Rods and the electrochromic performance of $Ni(OH)_2/In_2O_3$-rod composite porous film. *Thin Solid Film.* **2021**, *734*, 138839. [CrossRef]
6. Kotok, V.; Kovalenko, V.; Nafeev, R.; Melnyk, O. Investigation of the characteristics of sulfurized electrochromic $Ni(OH)_2$-PVA films deposited on transparent substrates. *East.-Eur. J. Enterp. Technol.* **2022**, *1*, 24–30. [CrossRef]
7. Abd-Elsabour, M.; Alhamzani, A.; Abou-Krisha, M. Fabrication of novel nickel-modified electrodes and their application for methanol oxidation in fuel cell. *Ionics* **2022**, *28*, 1915–1925. [CrossRef]
8. Jiang, L.; Chen, J.; An, Y.; Han, D.; Chang, S.; Liu, Y.; Yang, R. Enhanced electrochemical performance by nickel-iron layered double hydroxides (LDH) coated on Fe_3O_4 as a cathode catalyst for single-chamber microbial fuel cells. *Sci. Total Environ.* **2020**, *745*, 141163. [CrossRef]

9. Djellali, M.; Kameche, M.; Kebaili, H.; Bouhent, M.; Benhamou, A. Synthesis of nickel-based layered double hydroxide (LDH) and their adsorption on carbon felt fibres: Application as low cost cathode catalyst in Microbial Fuel Cell (MFC). *Environ. Technol.* **2019**, *42*, 492–504. [CrossRef]
10. Zhang, R.; Ran, T.; Cao, Y.; Zhang, Q.; Dong, F.; Yang, G.; Zhou, Y. Surface hydrogen atoms promote oxygen activation for solar light-driven no oxidization over monolithic α-$Ni(OH)_2$/Ni foam. *Environ. Sci. Technol.* **2020**, *54*, 16221–16230. [CrossRef]
11. Qin, H.; Wei, X.; Ye, Z.; Liu, X.; Mao, S. Promotion of phenol electro-oxidation by oxygen evolution reaction on an active electrode for efficient pollution control and hydrogen evolution. *Environ. Sci. Technol.* **2022**, *56*, 5753–5762. [CrossRef] [PubMed]
12. Li, H.; Zhu, H.; Shi, Y.; Shang, H.; Zhang, L.; Wang, J. Vacancy-rich and porous NiFe-layered double hydroxide ultrathin nanosheets for efficient photocatalytic no oxidation and storage. *Environ. Sci. Technol.* **2022**, *56*, 1771–1779. [CrossRef]
13. Yang, H.Y.; Zhang, X.X.; Zhang, H.Y.; Huang, M.; Yin, S.; Zhang, Y.F.; Wang, J. How to fit a response current-concentration curve? part (II) : Synergy of heterogeneous PANI@$NI(OH)_2$/NF towards high performance glucose sensing and a general semi-empirical model. *J. Electroanal. Chem.* **2022**, *909*, 116164. [CrossRef]
14. Manjushree, S.; Adarakatti, P.; Udayakumar, V.; Almalki, A. Hexagonal cerium oxide decorated on β-$Ni(OH)_2$ nanosheets stabilized by reduced graphene oxide for effective sensing of H_2O_2. *Carbon Lett.* **2021**, *32*, 591–604. [CrossRef]
15. Yang, T.; Zhang, W.; Wu, J.; Zhao, K.; Liu, S.; Zhao, Y. Tailored design of $Ni(OH)_2$ nanocages internally decorated with CuS nanocages to mutually ameliorate electrocatalytic dynamics for highly sensitive glucose detection. *J. Electroanal. Chem.* **2022**, *907*, 115893. [CrossRef]
16. Cagnetta, G.; Zhang, K.; Zhang, Q.; Huang, J.; Yu, G. Augmented hydrogen production by gasification of ball milled polyethylene with $Ca(OH)_2$ and $Ni(OH)_2$. *Front. Environ. Sci. Eng.* **2019**, *13*, 11. [CrossRef]
17. Hayek, N.; Landman, A.; Halpern, Y.; Slobodkin, I.; Davydova, E.; Rothschild, A. Carbon-cloth-supported nickel hydroxide anodes for electrochemical–thermally-activated chemical (E-TAC) water splitting. *J. Mater. Chem. A* **2022**, *10*, 726–739. [CrossRef]
18. Zhang, L.; Wang, T.; Wu, H.; Wang, H.; Wang, F. Nickel hydroxide array coated with NiFe alloy nanosheets for overall mixed water splitting. *J. Alloys Compd.* **2022**, *918*, 165564. [CrossRef]
19. Paul, T.; Mesbahi, T.; Durand, S.; Flieller, D.; Uhring, W. Sizing of lithium-ion battery/supercapacitor hybrid energy storage system for forklift vehicle. *Energies* **2020**, *13*, 4518. [CrossRef]
20. Babar, P.; Unde, M.G.; Patil, R.J. Hybrid Energy Control for an Electric Vehicle Using Super Capacitor and Battery. In Proceedings of the 2022 3rd International Conference on Electronics and Sustainable Communication Systems (ICESC), Coimbatore, India, 17–19 August 2022. [CrossRef]
21. Mishra, D.; Zhou, R.; Hassan, M.; Hu, J.; Gates, I.; Mahinpey, N.; Lu, Q. Bitumen and asphaltene derived nanoporous carbon and nickel oxide/carbon composites for supercapacitor electrodes. *Sci. Rep.* **2022**, *12*, 4095. [CrossRef]
22. Yu, X.-H.; Zhao, Z.-Y.; Yi, J.-L.; Liu, S.; Zhang, R.-L.; Wang, F.-Y.; Liu, L. Facile assembly of cobalt-nickel double hydroxide nanoflakes on nitrogen-doped hollow carbon spheres for high performance asymmetric supercapacitors. *J. Alloys Compd.* **2022**, *918*, 165551. [CrossRef]
23. Khedulkar, A.P.; Dang, V.D.; Pandit, B.; Bui, T.A.N.; Tran, H.L.; Doong, R.-A. Flower-like nickel hydroxide@tea leaf-derived biochar composite for high-performance supercapacitor application. *J. Colloid Interface Sci.* **2022**, *623*, 845–855. [CrossRef] [PubMed]
24. Liang, M.; Li, X.; Kang, Y.; RehmanLashari, N.U.; Zhang, X.; Zhao, Y.; Wang, H.; Miao, Z.; Fu, C. Ni-doped tin disulfide@Nickel hydroxide as robust cathode toward durable supercapacitor and aqueous Ni-Zn battery. *J. Power Sources* **2022**, *535*, 231486. [CrossRef]
25. Kachina, E.; Ivanova, N.; Zakharov, Y.; Simenyuk, G.; Ismagilov, Z.; Lomakin, M. Electrochemical Properties of the Composites Based on Multiwall Carbon Nanotubes Modified with Nanoparticles of Mixed Cobalt and Nickel Hydroxides. *Eurasian Chem. J.* **2022**, *24*, 115–121. [CrossRef]
26. Zhang, M.; Zang, R.; Zhang, M.; Liu, R.; Zhu, X.; Li, X.; Cui, H.; Zhu, H. Promoting the cyclic and rate performance of nickel hydroxide with ZnO via electrodeposition for supercapacitor. *J. Alloys Compd.* **2022**, *911*, 164865. [CrossRef]
27. Wiston, B.R.; Dhivyaprasath, K.; Tewatia, S.; Ashok, M. Optimization of nickel manganese ratio to attain highly efficient electroactive composite for supercapacitors. *J. Alloys Compd.* **2023**, *935*, 167982. [CrossRef]
28. Erdemutu, E.; Bai, C.; Ding, L. Electrospun Ni-$Ni(OH)_2$/Carbon Nanofibers as Flexible Binder-Free Supercapacitor Electrode with Enhanced Specific Capacitance. *J. Electron. Mater.* **2020**, *49*, 7211–7218. [CrossRef]
29. Nath, A.R.; Madhu, B.; Mohan, A.; Sandhyarani, N. Enhancing the stability of electrochemical asymmetric supercapacitor by incorporating thiophene-pyrrole copolymer with nickel sulfide/nickel hydroxide composite. J. *Energy Storage* **2021**, *46*, 103833. [CrossRef]
30. Boruah, B.D.; Misra, A. Nickel hydroxide coated carbon nanoparticles mediated hybrid three-dimensional graphene foam assembly for supercapacitor. *RSC Adv.* **2016**, *6*, 36307–36313. [CrossRef]
31. Wang, M.; Feng, Y.; Zhang, Y.; Li, S.; Wu, M.; Xue, L.; Zhao, J.; Zhang, W.; Ge, M.; Lai, Y.; et al. Ion regulation of hollow nickel cobalt layered double hydroxide nanocages derived from ZIF-67 for High-Performance supercapacitors. *Appl. Surf. Sci.* **2022**, *596*, 153582. [CrossRef]
32. Kapu, S.G.; Guddeti, P.R.; Sambasivam, S.; Yakkate, S.R.; Joo, S.W.; Pallavolu, M.R. Facile fabrication of hexagonal $Ni(OH)_2$ nanoparticles anchored g-C_3N_4 layered nanocomposite electrode material for energy storage applications. *Diam. Relat. Mater.* **2022**, *129*, 109376. [CrossRef]

33. Wang, G.; Qi, K.; Yan, Z.; Yue, L.; Ding, Y.; Li, W.; Xu, Z. Microwave hydrothermal synthesis of La decorated $Ni(OH)_2$ nanosheets for performance-enhanced hybrid supercapacitor. *Appl. Surf. Sci.* **2022**, *592*, 153293. [CrossRef]
34. Liu, J.; Han, E.; He, Y.; Tong, X.; Guo, S. Effect of soft template on nickel-cobalt layered double hydroxides grown on nickel foam as battery-type electrodes for hybrid supercapacitors. *Ionics* **2021**, *27*, 3129–3141. [CrossRef]
35. Tian, Y.; Zhu, L.; Shang, M.; Han, E.; Song, M. Effect of soft templating agent on NiCoAl-LDHs grown in situ on foamed nickel for high-performance asymmetric supercapacitors. *Ionics* **2019**, *26*, 1431–1442. [CrossRef]
36. Liu, J.; Han, E.; He, Y.; Yang, X.; Qiao, S.; Tong, X.; Tian, Y.; Gao, L. Effect of soft template on NiMn-LDH grown on nickel foam for battery-type electrode materials. *Ionics* **2021**, *27*, 1451–1463. [CrossRef]
37. Yedluri, A.K.; Kim, H.-J. Wearable super-high specific performance supercapacitors using a honeycomb with folded silk-like composite of $NiCo_2O_4$ nanoplates decorated with $NiMoO_4$ honeycombs on nickel foam. *Dalton Trans.* **2018**, *47*, 15545–15554. [CrossRef]
38. Arbi, H.M.; Yadav, A.A.; Kumar, Y.A.; Moniruzzaman; Alzahmi, S.; Obaidat, I.M. Polypyrrole-Assisted Ag Doping Strategy to Boost $Co(OH)_2$ Nanosheets on Ni Foam as a Novel Electrode for High-Performance Hybrid Supercapacitors. *Nanomaterials* **2022**, *12*, 3982. [CrossRef]
39. Neto, N.A.; Silva, J.; Tranquilin, R.; Longo, E.; Bomio, M.; Motta, F. Stabilization of the γ-Ag_2WO_4 metastable pure phase by coprecipitation method using polyvinylpyrrolidone as surfactant: Photocatalytic property. *Ceram. Int.* **2020**, *46*, 14864–14871. [CrossRef]
40. Lam, S.-M.; Kee, M.-W.; Sin, J.-C. Influence of PVP surfactant on the morphology and properties of ZnO micro/nanoflowers for dye mixtures and textile wastewater degradation. *Mater. Chem. Phys.* **2018**, *212*, 35–43. [CrossRef]
41. Kotok, V.; Kovalenko, V.; Mikolasek, M.; Ondrejka, P.; Zima, O.; Anataichuk, I.; Vodopyan, D.; Sukhyy, K. Characteristics investigation of composite electrochromic films based on $Ni(Oh)_2$, polyvinyl alcohol, and polyvinylpyrrolidone. *East.-Eur. J. Enterp. Technol.* **2022**, *3*, 58–65. [CrossRef]
42. Kotok, V.; Kovalenko, V. A study of the influence of polyvinyl pyrrolidone concentration in the deposition electrolyte on the properties of electrochromic $Ni(OH)_2$ films. *East.-Eur. J. Enterp. Technol.* **2020**, *4*, 31–37. [CrossRef]
43. Snook, G.A.; Duffy, N.W.; Pandolfo, A.G. Evaluation of the effects of oxygen evolution on the capacity and cycle life of nickel hydroxide electrode materials. *J. Power Sources* **2007**, *168*, 513–521. [CrossRef]
44. Kotok, V.; Kovalenko, V.; Malyshev, V. Comparison of oxygen evolution parameters on different types of nickel hydroxide. *East.-Eur. J. Enterp. Technol.* **2017**, *5*, 12–19. [CrossRef]
45. Chen, J.; Bradhurst, D.H.; Dou, S.X.; Liu, H.K. Nickel Hydroxide as an Active Material for the Positive Electrode in Rechargeable Alkaline Batteries. *J. Electrochem. Soc.* **1999**, *146*, 3606–3612. [CrossRef]
46. Oshitani, M.; Takayama, T.; Takashima, K.; Tsuji, S. A study on the swelling of a sintered nickel hydroxide electrode. *J. Appl. Electrochem.* **1986**, *16*, 403–412. [CrossRef]
47. Kovalenko, V.; Kotok, V. Anionic carbonate activation of layered (α + β) nickel hydroxide. *East.-Eur. J. Enterp. Technol.* **2019**, *3*, 44–52. [CrossRef]
48. Chang, Z.; Tang, H.; Chen, J.G. Surface modification of spherical nickel hydroxide for nickel electrodes. *Electrochem. Commun.* **1999**, *1*, 513–516. [CrossRef]
49. Pralong, V.; Delahaye-Vidal, A.; Beaudoin, B.; Leriche, J.; Tarascon, J. Electrochemical Behavior of Cobalt Hydroxide Used as Additive in the Nickel Hydroxide Electrode. *J. Electrochem. Soc.* **2000**, *147*, 1306–1313. [CrossRef]
50. Andrade, T.M.; Danczuk, M.; Anaissi, F.J. Effect of Precipitating Agents on the Structural, Morphological, and Colorimetric Characteristics of Nickel Hydroxide Particles. *Colloid Interface Sci. Commun.* **2018**, *23*, 6–13. [CrossRef]
51. Hu, C.-W.; Yamada, Y.; Yoshimura, K. Fabrication of nickel oxyhydroxide/palladium (NiOOH/Pd) nanocomposite for gasochromic application. *Sol. Energy Mater. Sol. Cells* **2018**, *177*, 120–127. [CrossRef]
52. Kumar, Y.A.; Das, H.T.; Guddeti, P.R.; Nallapureddy, R.R.; Pallavolu, M.R.; Alzahmi, S.; Obaidat, I.M. Self-Supported Co_3O_4@Mo-Co_3O_4 Needle-like Nanosheet Heterostructured Architectures of Battery-Type Electrodes for High-Performance Asymmetric Supercapacitors. *Nanomaterials* **2022**, *12*, 2330. [CrossRef] [PubMed]
53. Shruthi, B.; Madhu, B.; Raju, V.B.; Vynatheya, S.; Devi, B.; Jayashree, G.; Ravikumar, C. Synthesis, spectroscopic analysis and electrochemical performance of modified β-nickel hydroxide electrode with CuO. *J. Sci. Adv. Mater. Devices* **2017**, *2*, 93–98. [CrossRef]
54. Lyons, M.; Doyle, R.L.; Godwin, I.; O'Brien, M.; Russell, L. Hydrous Nickel Oxide: Redox Switching and the Oxygen Evolution Reaction in Aqueous Alkaline Solution. *J. Electrochem. Soc.* **2012**, *159*, H932–H944. [CrossRef]
55. Qin, R.; Pan, Y.; Duan, Z.; Su, H.; Ren, K.; Wang, W.; Li, Y.; Xi, N.; Wang, Y.; Zhang, L.; et al. Achieving High Stability and Rate Performance Using Spherical Nickel-Zinc Layered Double Hydroxide in Alkaline Solution. *J. Electrochem. Soc.* **2021**, *168*, 070539. [CrossRef]
56. Kotok, V.; Kovalenko, V. Definition of the influence of obtaining method on physical and chemical characteristics of Ni (OH)2 powders. *East.-Eur. J. Enterp. Technol.* **2019**, *1*, 21–27. [CrossRef]
57. Conway, B.; Birss, V.; Wojtowicz, J. The role and utilization of pseudocapacitance for energy storage by supercapacitors. *J. Power Sources* **1997**, *66*, 1–14. [CrossRef]
58. Wang, D.; Wei, A.; Tian, L.; Mensah, A.; Li, D.; Xu, Y.; Wei, Q. Nickel-cobalt layered double hydroxide nanosheets with reduced graphene oxide grown on carbon cloth for symmetric supercapacitor. *Appl. Surf. Sci.* **2019**, *483*, 593–600. [CrossRef]

59. Zhao, B.; Zhang, B.; Lu, C.; Cai, Z.; Li, L. Hierarchical hollow nanocages of Ni–Co amorphous double hydroxides for high-performance asymmetric supercapacitors. *J. Alloys Compd.* **2020**, *833*, 155130. [CrossRef]
60. Bao, Y.; Deng, Y.; Wang, M.; Xiao, Z.; Wang, M.; Fu, Y.; Guo, Z.; Yang, Y.; Wang, L. A controllable top-down etching and in-situ oxidizing strategy: Metal-organic frameworks derived α-Co/$Ni(OH)_2$@Co_3O_4 hollow nanocages for enhanced supercapacitor performance. *Appl. Surf. Sci.* **2019**, *504*, 144395. [CrossRef]
61. Zhang, D.; Guo, X.; Tong, X.; Chen, Y.; Duan, M.; Shi, J.; Jiang, C.; Hu, L.; Kong, Q.; Zhang, J. High-performance battery-type supercapacitor based on porous biocarbon and biocarbon supported Ni–Co layered double hydroxide. *J. Alloys Compd.* **2020**, *837*, 155529. [CrossRef]
62. Al Kiey, S.A.; Hasanin, M.S. Green and facile synthesis of nickel oxide-porous carbon composite as improved electrochemical electrodes for supercapacitor application from banana peel waste. *Environ. Sci. Pollut. Res.* **2021**, *28*, 66888–66900. [CrossRef] [PubMed]
63. Wang, P.; Zhou, H.; Meng, C.; Wang, Z.; Akhtar, K.; Yuan, A. Cyanometallic framework-derived hierarchical Co_3O_4-NiO/graphene foam as high-performance binder-free electrodes for supercapacitors. *Chem. Eng. J.* **2019**, *369*, 57–63. [CrossRef]
64. Kishore, S.C.; Atchudan, R.; Edison, T.N.J.I.; Perumal, S.; Alagan, M.; Vinodh, R.; Shanmugam, M.; Lee, Y.R. Solid Waste-Derived Carbon Fibers-Trapped Nickel Oxide Composite Electrode for Energy Storage Application. *Energy Fuels* **2020**, *34*, 14958–14967. [CrossRef]
65. Karuppaiah, M.; Sakthivel, P.; Asaithambi, S.; Murugan, R.; Babu, G.A.; Yuvakkumar, R.; Ravi, G. Solvent dependent morphological modification of micro-nano assembled Mn_2O_3/NiO composites for high performance supercapacitor applications. *Ceram. Int.* **2018**, *45*, 4298–4307. [CrossRef]
66. AshokC, S.; Thomas, N. Influence of fuel to oxidizer ratio on the supercapacitive properties of NiO synthesized by solution combustion method. *Solid State Sci.* **2022**, *133*, 107004. [CrossRef]
67. Moniruzzaman; Kumar, Y.A.; Pallavolu, M.R.; Arbi, H.M.; Alzahmi, S.; Obaidat, I.M. Two-Dimensional Core-Shell Structure of Cobalt-Doped@MnO_2 Nanosheets Grown on Nickel Foam as a Binder-Free Battery-Type Electrode for Supercapacitor Application. *Nanomaterials* **2022**, *12*, 3187. [CrossRef]